

APPLICATION OF AN ELLIPSOIDAL HEART MODEL IN STUDYING LEFT VENTRICULAR CONTRACTIONS

J. H. J. M. VAN DEN BROEK and M. H. L. M. VAN DEN BROEK

Department of Medical and Physiological Physics, University of Utrecht,
Sorbonnelaan 4, Utrecht, The Netherlands

Abstract – A geometrical model for the left ventricle is developed consisting of a nested set of truncated ellipsoidal shells of revolution. The geometrical parameters are modelled with the aid of measuring data and assumptions about ventricular deformation. The shells contain muscle fibres which generate wall tension (according to a muscle model previously described), from which ventricular pressure results. Fibre length and orientation have different values per shell. After ventricular deformation (change in preload, ejection) new values of the length and orientation can be calculated.

The geometrical aspects of the model were tested with literature data. Apart from the apical region the results appear to be satisfactory. Calculated fibre lengths over the wall agree reasonably with measured data, if rather realistic ventricular shape changes were applied. The mechanical aspects (pressure generation, developed flow) were also tested with experiments on rabbit hearts. They agree with previous results obtained from a cylindrical model.

INTRODUCTION

In a previous study (van den Broek and Denier van der Gon, 1980b) a model which could be applied to both isovolumic and non-isovolumic left ventricular contractions was developed. Contractile properties were based on the sliding filament muscle theory. Special attention was paid to the influence of physiologically relevant contraction parameters on pressure generation and flow. In order not to obscure relevant mechanisms a relatively simple model for the ventricular geometry was used: a thick-walled cylinder. Such a model can give a rather good approximation of the ventricle in its equatorial region (Back, 1977). The model did contain relevant features such as fibre orientation and sarcomere length distribution over the wall. Also shape changes during the various phases of contraction were allowed. The model was tested with the help of data obtained from experiments on isolated rabbit hearts. One of the conclusions was that for an accurate evaluation of ventricular pressure, ventricular dimensions are important parameters. They should be measured simultaneously with pressure and flow. To incorporate these in this study, the model is improved by using a thick-walled truncated ellipsoid of revolution with non-uniform wall-thickness (See also van den Broek and Denier van der Gon, 1980a.) The use of such a model is suggested by Streeter and Hanna (1973a,b). Ellipsoidal models give a better overall approximation of the ventricle (Back, 1977). Furthermore, measured dimensions can be introduced more significantly in an ellipsoidal model than in a cylindrical or spherical model. This holds in particular for measurements done with ultrasonic techniques,

which are in vogue more and more and by which the lengths of ventricular "axes" are measured (Suga and Sagawa, 1974; Günterth, 1974; Sasayama *et al.*, 1976; Rankin *et al.*, 1976). The axes so found can be used directly as estimates of the axes of ellipsoids describing ventricular inner and outer walls.

Thick-walled ellipsoidal heart models, the walls of which consist of muscle fibres, have been reported previously. Streeter *et al.* (1970) used force-length data from papillary muscle to calculate static fibre stress and resulting pressure. Wong (1973) used a muscle model based on the Huxley (1957) theory to simulate isovolumic pressure development. The model developed by us was tested against data available in the literature. Furthermore, a comparison with the previously developed cylindrical model (van den Broek and Denier van der Gon, 1980b) was made by fitting the model to the same experiments (pressure development in rabbit hearts) as to which the cylindrical model was fitted.

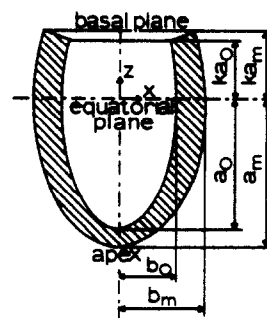


Fig. 1. Longitudinal section of the ellipsoidal geometry, showing the important geometrical parameters.

Received 25 June 1979.

VENTRICULAR MODEL

Modelling procedure

The ventricular model consists of a hollow truncated ellipsoid (see Fig. 1). The wall of the ventricle is divided into m layers by means of $m + 1$ ellipsoids E_i ($i = 0, 1, \dots, m$). E_0 represents the endocardium and E_m the epicardium. The (semi-)* axes of E_i coincide with the x , y and z directions and they are denoted b_i , b_i and a_i respectively with $a_i > b_i$. E_i now satisfies the equation

$$\frac{x^2}{b_i^2} + \frac{y^2}{b_i^2} + \frac{z^2}{a_i^2} = 1, \quad (1)$$

and is truncated at the intersection with the plane $z = ka_i$, where k is a constant having the same value for each ellipsoid (see Fig. 1). The geometry described in this way is completely determined by five parameters, e.g. the short and long endocardium axes b_0 and a_0 , the short and long epicardium axes b_m and a_m , and the factor k .

The muscle fibres in the wall lie parallel to the surface of the ellipsoids E_i at an angle ϕ with the circumference. This angle is different in different wall layers (Streeter *et al.*, 1969; Ross and Streeter, 1975). Also the length of the fibres in the wall may differ in each layer (Hort, 1960; Spotnitz *et al.*, 1966; Yoran *et al.*, 1973). In the apex the fibre orientation is not defined. For this reason the pressure in the apex is calculated in a point very near to the apex.

To eliminate the influence of the spread of excitation over the ventricle it is supposed that all fibres contract simultaneously. Therefore in our experiments synchronous stimulation was applied. This probably also reduces torsion and isovolumic shape changes of the ventricle. Besides, it is supposed that no bending along the z -axis or peristaltic contraction is present. The ventricle will always remain ellipsoidal, but its eccentricity however, may change due to ejection or a change in preload.

Determination of ventricular pressure

To calculate the pressure it is supposed that shear stresses may be neglected at least during the active

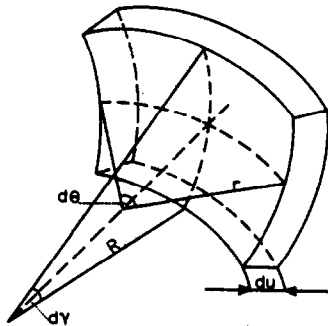


Fig. 2. The radii of curvature of a small element of the wall.

phase (van den Broek and Denier van der Gon, 1980b), as well as the influence of wall acceleration and pressure gradients in the ventricle during ejection (Back, 1977).

The pressure difference dp over a thin layer of the wall with thickness du is given by (Mirsky, 1970):

$$dp = \left(\frac{\sigma_{\theta\theta}}{r} + \frac{\sigma_{\gamma\gamma}}{R} \right) du, \quad (\text{see Fig. 2}) \quad (2)$$

where $\sigma_{\theta\theta}$ and $\sigma_{\gamma\gamma}$ are local wall stresses (minus a hydrostatic pressure) in the θ (circumferential) and γ (longitudinal) direction respectively. r is the radius of curvature in a plane through the normal to the wall and a tangent parallel to the x - y plane. R is the radius of curvature through the normal and the z -axis.

Active muscle stress σ_m is generated by the muscle fibres, making an angle ϕ with the circumferential direction

$$\sigma_{\theta\theta} = \sigma_m \cos^2 \phi \quad \text{and} \quad \sigma_{\gamma\gamma} = \sigma_m \sin^2 \phi. \quad (3)$$

σ_m will be expressed in the muscle force F_m , the length l_m and volume VM of the fibre

$$\sigma_m = \frac{F_m l_m}{VM}. \quad (4)$$

F_m follows from the muscle model (van den Broek and Denier van der Gon, 1980b); VM is supposed to be constant.

From equations (2-4) it follows that the pressure difference P between endo- and epicardium in a certain point S on the endocardium becomes:

$$P(S) = \frac{1}{VM} \int_{\text{wall}} F_m(u) l_m(u) \times \left\{ \frac{\cos^2 \phi(u)}{r(u)} + \frac{\sin^2 \phi(u)}{R(u)} \right\} du, \quad (5)$$

where u is the coordinate along the normal N to the inner wall in S . In general N is not exactly perpendicular to the outer wall. However, the error in the pressure introduced by this approximation appears to be very small.

Equation (5) holds not only for an ellipsoid of revolution, but also for a general ellipsoid. However, it can be proved (see Appendix A) that in the latter case the pressure along meridians converges to different values when approaching the apex.

The integral in equation (5) is approximated by a sum over the m wall layers. In each layer the value of the integrand is taken at the middle of that layer:

$$P(S) \approx \frac{1}{VM} \sum_{i=1}^m F_{m,i} l_{m,i} \left\{ \frac{\cos^2 \phi_i}{r_i} + \frac{\sin^2 \phi_i}{R_i} \right\} \Delta u_i; \quad (6)$$

Δu_i is the length along N between E_{i-1} and E_i .

In one ventricular geometry (the reference situation) the wall is divided into m layers by $m + 1$ equidistant ellipsoids. In each layer $l_{m,i}$ and ϕ_i are supposed to be known. Within one layer they are taken to be constant. $P(S)$ can be calculated with the aid of $F_{m,i}$ which follows from the muscle model, together with r_i and R_i .

* In all cases axes mean semi-axes.

When ventricular dimensions have changed and the new values of the five parameters describing the geometry are determined, the new coordinates of S and the direction of N can be calculated. The new ellipsoids E_i and new values of Δu_i follow from the assumption that the volume of each wall layer remains constant.

In order to calculate new fibre length and orientation it is supposed that the fibres lie within tangent planes on ellipsoids going through the middle of each layer. New values of $l_{m,i}$ and ϕ_i can be calculated from the transformation of two mutually perpendicular vectors in the tangent planes. These calculations are further elaborated in Appendix B, where expressions for r_i and R_i are also given.

Determination of ventricular geometry

Several methods are described in the literature for measuring ventricular dimensions (see review of Sandler and Alderman, 1974). Some of the most reliable ones are angiographic methods (Sandler, 1970) and ultrasonic methods. In the latter case transit time is measured with the aid of ultrasonic transducers (Suga and Sagawa, 1974; Günterth, 1974; Sasayama *et al.*, 1976; Rankin *et al.*, 1976). In our experiments with isolated rabbit hearts the use of ultrasonic techniques did not give reliable results. This was mainly due to the fact that rabbit hearts are relatively small with regard to the transducers. The wall was seriously damaged, when the transducers were sutured in place. With the aid of other measurable quantities, literature data and some assumptions about ventricular deformation, an estimation of the five parameters necessary to define the ellipsoid may also be obtained. These conditions, imposed in the reference situation and after ventricular deformation (other preloads, ejection phase), will be discussed below.

I. *Reference situation.* For the reference situation (i.e. the situation at one specified preload with given values of $l_{m,i}$ and ϕ_i) the following conditions are used (see Fig. 3):

1. The model inner volume V_0 is equal to a value obtained from own experiments, e.g. by emptying the heart, or from literature data. V_0 is defined as:

$$V_0 = V(E_0) - V_q + V_e, \quad (7)$$

where $V(E_0)$ is the volume enclosed by the ellipsoid E_0 , V_q is the papillary muscle volume, V_e is the small extra

volume resulting from the special way of truncating the ellipsoid (see Appendix B, equation A5 for $i=m$). V_q is estimated from literature data.

2. Wall volume V_w of the model is equal to a value obtained by weighing the ventricular wall, or from literature data. V_w is defined as:

$$V_w = V(E_m) - V(E_0) - V_e + V_q, \quad (8)$$

where $V(E_m)$ is the volume enclosed by E_m .

3. The ratio d between the axes of E_0 is obtained from literature data and defined as:

$$d = b_0/a_0. \quad (9)$$

4. The truncation factor k is obtained from the literature.

5. The pressure drop over the apical wall (site A) has to equal the pressure drop over the equatorial wall (site E).

With condition 5 equal pressures are obtained at at least two endocardial points. Theoretically, the pressure should be identical at every point. It will be checked how far an ellipsoid of revolution meets this requirement. When using condition 5 the time course of the pressure and the exact value of the pressure are of no importance. For this reason a simple static muscle model for calculating the pressure can be applied. In the chosen muscle model muscle force is directly related to sarcomere length by applying a force-length relation as measured by Pollack and Krueger (1974).

A numerical procedure for determining the axes with the conditions described above is given in Appendix C.

II. *Situation at new preloads and during ejection.* After ventricular deformation it is assumed that V_w and k remain the same as in the reference situation (condition 2 and 4). In condition 1, V_0 should be replaced by V_p (the volume at a new preload) or by $V(t)$ (the volume during ejection). To account for the influence of ventricular shape (determined by d in our model), condition 3 is replaced by a condition in which d depends linearly on ventricular volume:

$$d = d_r \left(1 + \frac{V_p - V_0}{V_0} d_p + \frac{V - V_p}{V_0} d_e \right), \quad (10)$$

where d_r is the value of d in the reference situation, the parameters d_p and d_e represent the influence of a preload change and ejection on d respectively.

By varying d_p and d_e the influence of shape changes can be tested. An impression of d_p cannot be obtained from the literature, since the influence of preload on ventricular shape has not yet been reported. With regard to the ejection phase, literature data show that in particular the short axes shorten, while the long axes remain nearly constant (Streeter and Hanna, 1973a; Ross *et al.*, 1967).

When the condition for equal pressures at two sites (condition 5) is maintained, the model results (e.g. simulated sarcomere length distributions over the wall) do not give good agreement with literature data

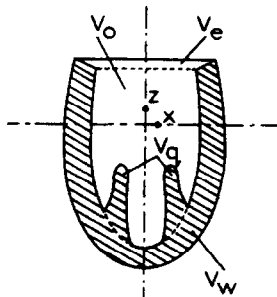


Fig. 3. Longitudinal section of the ellipsoidal geometry, showing the different volume compartments.

Table 1. Sarcomere lengths across the left ventricular wall at different preloads

Situation	End-diastolic pressure	End-diastolic volume	Endocardium		Sarcomere lengths (μm) in 10 wall layers										Epicardium
					1	2	3	4	5	6	7	8	9	10	
	mmHg	cm^3													
1	2	25.0	1.82	1.92	2.02	2.07	2.05	2.04	2.03	2.01	1.99	1.97			
2	6	37.0	1.95	2.05	2.14	2.12	2.10	2.08	2.07	2.06	2.05	2.04			
3	12	53.4	2.06	2.14	2.23	2.27	2.24	2.22	2.21	2.20	2.19	2.18			
4	20	62.0	2.30	2.30	2.29	2.29	2.28	2.28	2.27	2.27	2.26	2.26			

(see results). Better results are obtained when ventricular deformation is specified more accurately.

We revise condition 5 as follows:

If ventricular preload has changed, it is supposed that the ratio between the wall thickness at the apex h_A and the wall thickness at the equator h_E remains the same as in the reference situation. This assumption cannot be checked yet because of lack of suitable literature data. However, as a first approximation, this assumption does not seem to be unrealistic. During ejection, h_A is supposed to remain constant. This is in agreement with the literature (Streeter and Hanna, 1973a).

It will be checked how much the pressures at different endocardial points diverge from one another when using this new condition 5.

The numerical procedures for determining the axes with the new conditions given above are represented in Appendices D and E.

RESULTS

Simulations using literature data of dog hearts

Simulations under various conditions were carried out to investigate the features and limitations of the ellipsoidal heart model. We will make use of the detailed measurements of sarcomere length distributions over the wall as given by Yorán *et al.* (1973). In their study the (equatorial) wall was divided into five

layers, in which sarcomere lengths were measured at different end-diastolic pressures. For our simulations we interpolated these data to ten wall layers (see Table 1). Furthermore, we converged the given end-diastolic pressures to end-diastolic volumes by using a passive pressure-volume relation given by Spotnitz *et al.* (1966) obtained in similar experiments. Useful data about ventricular geometry of dog hearts are given by Streeter and Hanna (1973a), for one end-diastolic volume of 52.4 cm^3 and one end-systolic volume of 20.6 cm^3 (see Table 2 situation M_d and M_s respectively). They got their data from experiments by Ross *et al.* (1967) who used techniques for rapid fixation of left ventricles.

Reference situation

The ventricular axes belonging to the end-diastolic volume of 52.4 cm^3 will be calculated with the procedure for determining the reference situation (see ventricular model). In the calculations the values for k , V_w and V_q are taken as the average between the values given in the situations M_d and M_s of Table 2. The sarcomere length distribution is obtained from situation 3 of Table 1. The fibre orientation values are adopted from Streeter *et al.* (1966). The fibre angle is supposed to vary linearly from 60° (inner wall) to -60° (outer wall). In Table 2 the calculated axes are represented in situation C_d . The table shows that the calculated inner axes correspond better to the experiments than the outer axes. This can be expected since the ratio d between the measured inner axes was used in the simulations. It further follows that the calculated wall thickness at the equator h_E is too large, while the one at the apex is too small. This probably means that

Table 2. Measured and calculated end-diastolic and end-systolic data

		M_d	C_d	M_s	C_s
b_0	cm	1.91	1.90	1.37	1.29
b_m	cm	2.84	3.02	2.58	2.78
a_0	cm	4.18	4.15	4.01	3.78
a_m	cm	4.74	4.64	4.52	4.26
h_E	cm	0.93	1.12	1.21	1.49
h_A	cm	0.56	0.49	0.51	0.49
d		0.46	0.46	0.34	0.34
k		0.45	0.48	0.51	0.48
V_0	cm^3	52.4	52.4	20.6	20.6
V_w	cm^3	94.0	94.4	94.8	94.4
V_q	cm^3	2.4	2.6	2.8	2.6

The columns M_d and M_s represent literature data at one end-diastolic and one end-systolic volume. The values for h_E , h_A and d are calculated from the axes.

In the columns C_d and C_s the calculated end-diastolic and end-systolic axes are represented, from which h_E and h_A directly follow. The remaining parameters are used as input data.

Table 3. Influence of input data on the calculated axes in the reference geometry

b_0	b_m	a_0	a_m	Variation with regard to situation C_d of Table 2
cm	cm	cm	cm	
1.90	3.02	4.15	4.64	
1.90	3.02	4.16	4.61	$\phi_0 = 75^\circ$; $\phi_m = -75^\circ$
1.90	3.01	4.15	4.66	$\phi_0 = 52^\circ$; $\phi_m = -52^\circ$
1.90	3.02	4.15	4.63	$l_{m,i} = l_{m,i} + 0.06 \mu\text{m}$
1.90	3.02	4.15	4.65	$l_{m,i} = l_{m,i} - 0.06 \mu\text{m}$
1.86	3.03	4.08	4.59	$V_q = 0.0 \text{ cm}^3$
1.93	3.00	4.22	4.68	$V_q = 5.2 \text{ cm}^3$
1.87	3.00	4.11	4.59	$k = 0.53$
1.91	3.04	4.19	4.68	$k = 0.44$
1.83	2.94	4.45	4.88	$d_0 = 0.41$
1.95	3.09	3.87	4.42	$d_0 = 0.51$

Table 4. Calculated values of $\overline{\Delta s}$, ratio h_A/h_E and P at different preloads for different values of d using equal pressures at site E and A

$d \rightarrow$		0.410	0.435	0.460	0.485
V_p (cm ³) ↓	$\overline{\Delta s}$ (μm)	0.239	0.241	0.244	0.246
	h_A/h_E	0.444	0.470	0.497	0.524
	P	0.715	0.719	0.723	0.727
25	$\overline{\Delta s}$ (μm)	0.132	0.132	0.135	0.139
	h_A/h_E	0.405	0.431	0.457	0.483
	P	0.707	0.711	0.715	0.719
37	$\overline{\Delta s}$ (μm)	0.119	0.096	0.084	0.084
	h_A/h_E	0.368	0.393	0.418	0.443
	P	0.733	0.737	0.741	0.745
62	$\overline{\Delta s}$ (μm)	0.119	0.096	0.084	0.084
	h_A/h_E	0.368	0.393	0.418	0.443
	P	0.733	0.737	0.741	0.745

For the reference situation ($V_0 = 52.4$ cm³); $d_r = 0.460$; $h_A/h_E = 0.438$; $P = 0.748$.

$\overline{\Delta s}$ is the root mean square deviation between calculated and measured sarcomere lengths.

P is the developed pressure in arbitrary units, calculated at site E and A.

the real ventricle generates less stress in the apex than in the equator.

At an endocardial point M with coordinates ($b_0\sqrt{2}$, $0, b_0\sqrt{2}$) the pressure appears to be 0.15% lower than the pressure at the equator or apex. It follows that an ellipsoidal model is rather well suited to produce almost equal endocardial pressures. Several data have been varied to investigate the influence of input data in the procedure for the reference geometry (see Table 3). Variation of ϕ_i , $l_{m,i}$, V_q and k have little effect, in contrast to d , which directly determines the axes.

Other preloads

First it is investigated whether the requirement for equal pressures at two points on the inner wall (condition 5, reference situation) can also be used for the determination of geometries at other preloads. The calculations are done for preloads belonging to situations 1, 2 and 4 of Table 1, for several choices of the

axes ratio d . In all cases the same fibre orientation is applied as used in the reference geometry. Table 4 represents the wall thickness ratio of the calculated geometries as well as the calculated pressures. From the table it follows that rather different wall thickness ratios are found at different preloads. Furthermore, there is no clear increase in pressure at increasing preloads. It is now investigated how the sarcomere lengths in the equatorial wall change when the ventricle deforms from the reference geometry (52.4 cm³) to the geometries found above at other preloads, see Fig. 4a, b, c. To quantify these results the root mean square deviation $\overline{\Delta s}$ between the sarcomere length data of Yoran and the calculated data is determined and represented in Table 4. $\overline{\Delta s}$ appears to be very large compared with the measuring error in Yoran's data, which is smaller than 0.01 μm. Variation of d does not lead to any improvement.

Geometries are now determined by using the condition that ventricular wall thickness remains constant when deforming from the reference situation (new condition 5). Again several values for d are applied. The equatorial sarcomere length distributions are given in Fig. 5a, b, c. In Table 5 $\overline{\Delta s}$ is represented as well as the pressures calculated at three endocardial sites. $\overline{\Delta s}$ is significantly lower than in Table 4. There is also a clear pressure increase at increasing preloads. However, at 62 cm³ the equatorial pressure decreases again, because the sarcomere lengths have passed the maximum of the force-length relation. Yoran *et al.* (1973) still find a pressure increase at 62 cm³. From 25.0 cm³ to 52.4 cm³ they reported an increase in (developed) pressure of 29%, while our model predicts an increase in P_E of 25%. The table also shows that in general the pressure at the apex deviates most from the one at the other two sites. The lowest values of $\overline{\Delta s}$ are obtained when d increases at increasing preloads from 25.0 cm³ to 52.4 cm³, while at higher preloads d has to decrease again. This disposition to a more spherical shape at increasing preloads in the lower preload range

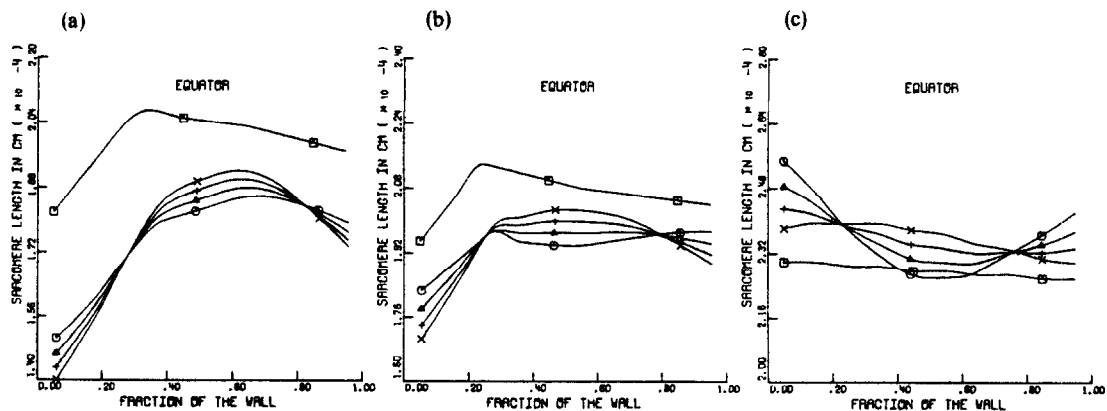


Fig. 4. Sarcomere length distributions in the equatorial wall, at end-diastolic volumes of 25.0 cm³ (a), 37.0 cm³ (b) and 62.0 cm³ (c). Measured lengths (Yoran) used for determining the geometry (□). Calculated length when deforming from the reference situation (52.4 cm³) to geometries obtained with $d = 0.410$ (○); $d = 0.435$ (Δ); $d = 0.460$ (+); $d = 0.485$ (x).

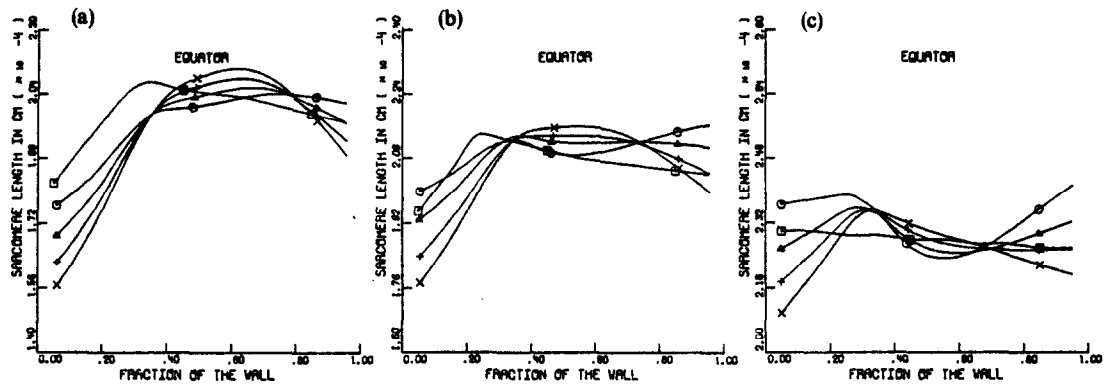


Fig. 5. Sarcomere length distributions in the equatorial wall, at end-diastolic volumes of 25.0 cm³ (a), 37.0 cm³ (b) and 62.0 cm³ (c). Measured lengths (Yoran) (□). Calculated length when deforming from the reference situation (52.4 cm³), with a constant wall thickness ratio h_A/h_E , for $d = 0.410$ (○); $d = 0.435$ (Δ); $d = 0.460$ (+); $d = 0.485$ (×).

is in agreement with calculations based on the equilibrium of forces acting in the z-direction of cylindrical heart models (Arts 1978; van den Broek and Denier van der Gon, 1980b).

From the table the value of d_p (equation 10) can be approximated by 0.20 for preloads lower than 52.4 cm³, and by -0.30 for higher preloads. So d_p is not a constant at every preload. With these values of d_p the sarcomere lengths across the wall are calculated over a wide range of end-diastolic volumes, at sites E, M and A (see Fig. 6a, b, c). The sarcomere lengths are almost the same in the midwall regions of the three sites. The lengths at site A differ from the other two sites particularly in the endocardial and epicardial regions. At preloads lower than 20 cm³ the endocardial sarcomere lengths become lower than the minimum length (1.65 μm) for cardiac muscle (Sonnenblick and Skelton, 1974). A rearrangement of sarcomeres in the endocardial wall region probably occurs at these low preloads. Spotnitz *et al.* (1966) measured sarcomere length at very low preloads. Their

data are not so accurate, since only three wall layers were used. At a preload of 13 cm³ (0 mmHg) they found equal sarcomere lengths of 1.92 μm in all wall layers. Our calculated lengths at site E agree in a large part of the wall (from wall fraction 0.4 to 1.0) with these data, within the measuring error (0.05 μm) (see Fig. 6a). The fibre orientation is hardly influenced by preload changes. If ϕ_0 and ϕ_m are chosen to be 60° and -60° respectively at a preload of 52.4 cm³, they become 62.2° and -57.8° at 25 cm³ and they become 58.9° and -59.9° at 62 cm³.

Ejection phase

The measured data in Table 2 show that the equatorial wall thickness h_E changes substantially as a result of ejection, while the apical wall thickness h_A remains reasonably constant. For this reason the end-systolic axes (C_S) are calculated under the condition that h_A remains constant during ejection. A value of $d_s = 0.42$ (equation 10) deducted from the table is used for the calculations. As can be seen from the table the end-systolic axes are modelled less adequately than the end-diastolic ones. The calculated sarcomere lengths at the three sites are represented in Fig. 7a, b, c as a function of the volume during ejection from 52.4 cm³ to 22.4 cm³. In the apex the endocardial sarcomere lengths differ greatly from the lengths at the other sites. Literature data are not available for comparison with these simulated values. During ejection the fiber angle ϕ_0 changes most (i.e. from 60.0° to 69.8°) while ϕ_m remains nearly the same (i.e. from -60.0° to 60.1°).

Simulations using own experimental data from rabbit hearts

The ellipsoidal model is also applied to simulate the same results for which the cylindrical model was tested (van den Broek and Denier van der Gon, 1980b). The muscle model that was used together with experimental methods and curve fitting procedures are given in van den Broek and Denier van der Gon (1980a, b). The results of one representative experiment are shown in this study.

Table 5. Calculated values of Δs and the pressure at three sites at different preloads, for various values of d . (The wall thickness ratio is supposed to remain constant ($h_A/h_E = 0.438$))

d		0.410	0.435	0.460	0.485
25	V_p (cm ³)				
	Δs (μm)	0.054*	0.071	0.094	0.118
	P_E	0.602	0.622	0.629	0.660
	P_M	0.610	0.611	0.622	0.631
	P_A	0.543	0.554	0.575	0.581
37	Δs (μm)	0.058	0.048	0.065	0.091
	P_E	0.680	0.701	0.710	0.733
	P_M	0.739	0.748	0.752	0.751
	P_A	0.662	0.673	0.670	0.682
	Δs (μm)	0.077	0.038	0.049	0.080
62	P_E	0.573	0.674	0.702	0.729
	P_M	0.701	0.799	0.818	0.831
	P_A	0.728	0.721	0.701	0.698

* This value of Δs is the minimum at this preload. At lower values of d , Δs increases.

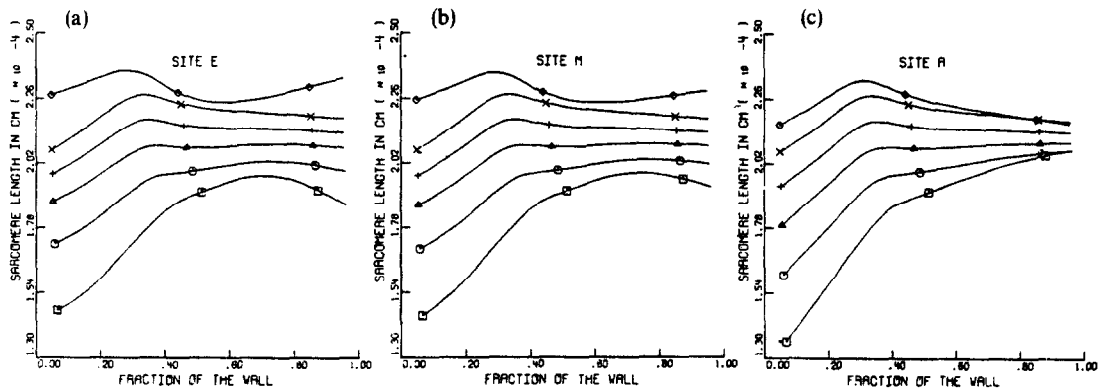


Fig. 6. Simulated sarcomere length distributions over a wide preload range at site E, M and A.

symbol	end-diastolic volume (cm ³)
□	13.0
○	23.0
△	33.0
+	43.0
×	53.0
◇	63.0

A preload of 0 mmHg is chosen as the reference situation. At this preload the sarcomere lengths measured by Spotnitz *et al.* (1966) are used ($l_{m,i} = 1.92 \mu\text{m}$). It is assumed that these data are also appropriate for rabbit hearts. The same is supposed to hold for the fibre orientation (chosen values $\phi_0 = 60^\circ$, $\phi_m = -60^\circ$). The other values chosen are: $V_0 = 1 \text{ cm}^3$; $V_w = 5 \text{ cm}^3$; $V_a = 0.01 \text{ cm}^3$; $d_r = 0.42$; $k = 0.50$. The calculated axes now become: $b_0 = 0.46 \text{ cm}$; $b_m = 1.10 \text{ cm}$; $a_0 = 1.10 \text{ cm}$; $a_m = 1.40 \text{ cm}$.

In the reference situation contraction parameters are fitted. With these parameters contractions at higher preloads and contractions with flow are simu-

lated. The measured and simulated isovolumic pressure curves at different preloads are given in Fig. 8. Figure 9 shows an isovolumic and a non-isovolumic contraction with an ejection fraction of 52%. All simulated pressures are calculated at site E. In the reference situation P_M appears to be 0.15% less than P_E . At a preload of 2 mmHg P_A is 2% lower than P_E , while during ejection at maximal flow P_A is 7% lower than P_E .

The simulation results are almost the same as those obtained with the cylindrical model. Again the use of a real or apparent series elastic element and a preload dependent activation seems to be necessary as well as

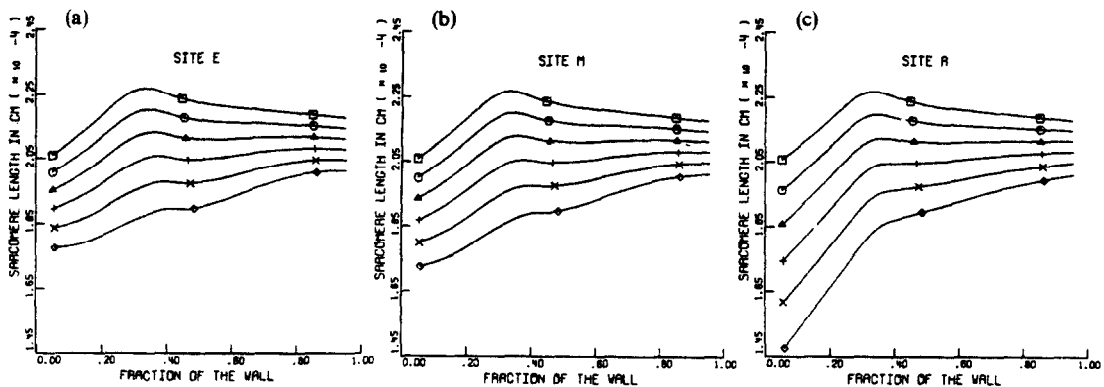


Fig. 7. Simulated sarcomere lengths throughout the wall at site E, M and A during ejection phase.

symbol	volume during ejection (cm ³)
□	52.4
○	46.4
△	40.4
+	34.4
×	28.4
◇	22.4

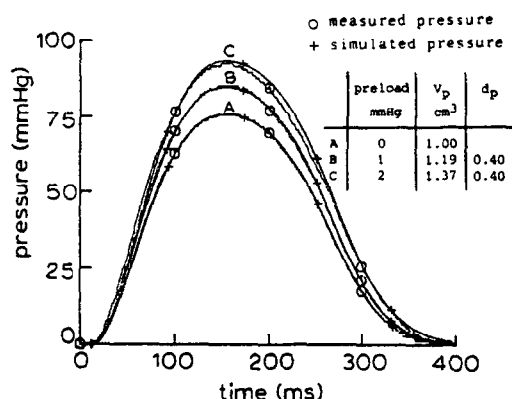


Fig. 8. Measured and simulated isovolumic pressure curves at different preloads. The measured tracings are not very smooth as a result of the analog-digital conversion.

ventricular shape changes. The best results are obtained if d_p and d_e are chosen to be 0.40 and 0.25 respectively.

DISCUSSION

As can be expected an ellipsoidal heart model leads to more complicated calculations for ventricular pressure development and ventricular deformation, than cylindrical or spherical models. Also more input data are required: a truncated ellipsoidal model is determined by five parameters, a cylindrical model by three and a spherical model only by two. Using ellipsoidal models special attention should be paid to the equality of endocardial pressures. In cylindrical or spherical models this requirement is always met. However, ellipsoidal models have the great advantage that they give a much better overall approximation of left ventricular geometry.

Rather complicated procedures have been developed in this study to determine the parameters describing the ellipsoidal geometry since these para-

meters are not usually directly available. The procedures can be simplified if more ventricular dimensions are measured. For instance, if ventricular outer axes are determined experimentally, (e.g. using ultrasonic methods) conditions 2 and 3 for the reference situation can be dropped.

The model was tested against meagre and incomplete literature data. In the reference situation the calculated apical wall thickness appears to be too small and the equatorial wall thickness too large (see Table 2). This phenomenon may be caused by the following facts:

The apical region cannot be described correctly with an ellipsoid of revolution.

The sarcomere lengths and/or the fibre orientations at site A and E differ substantially from one another. Fibres at site A generate lower forces than fibres at site E as a result of a different activation, perfusion etc.

The ratio between contractile and non-contractile tissue is lower at site A than at site E.

Although fibre orientation may change somewhat from the equator to the apex (Streeter *et al.*, 1969) it is certainly not enough to explain all the differences that are found.

During a preload change our simulations suggest that the condition for a constant wall thickness ratio between the apex and the equator results in calculated sarcomere length distributions as well as a calculated developed pressure-preload curve, which agree reasonably well with experiments. Not unrealistic shape changes have to be taken into account (see Table 4). As a disadvantage, different endocardial pressures are found. An explanation for these pressure differences (see Table 5), the differences between measured and calculated sarcomere lengths (see Fig. 5) as well as the very low endocardial lengths at low preloads (see Fig. 6) may be due to the fact that the real ventricular geometry deviates from an ellipsoid and that the assumed shape changes (equation 10) are too simple. In reality other kinds of deformation will also occur such as torsion, bending of the z-axis etc. Torsion (around the z-axis) in particular influences the sarcomere lengths in the endocardial and epicardial wall layers. The observed deviation between measured and calculated length were largest in these regions (see Fig. 5).

The calculated sarcomere lengths during ejection (see Fig. 7) could not be tested experimentally. The results show that in the apex the endocardial lengths become too small. This may be explained by the same facts as given above for a preload change.

In simulating the rabbit heart experiments the ellipsoidal model gives, as can be expected, about the same results as the cylindrical model, since both models present the same characteristics. Thus, for the present case, when ventricular dimensions are not exactly known the relatively simple cylindrical model is preferable for these simulations.

In general our calculations show that ventricular

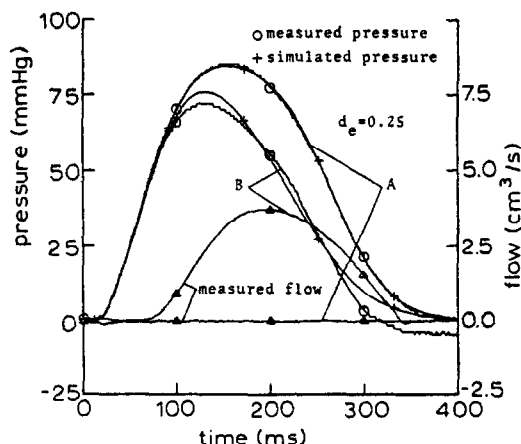


Fig. 9. Isovolumic (A) and non-isovolumic (B) contractions at a preload of 1 mmHg. The experimental flow curves do not resemble those measured *in vivo* experiments because of the use of a simple construction generating the afterload.

geometry and the way in which the ventricle deforms have a great influence on the results. More experimental data are needed. This holds also for anatomical data of the heart, such as fibre orientations and sarcomere length distributions. They should be measured at several ventricular sites (also the apex!) and at various end-diastolic and end-systolic volumes.

Acknowledgements – The authors wish to thank A. Crowe, J. J. Denier van der Gon, K. N. B. El Shuraydeh and E. A. Wolfs for their helpful criticism of this manuscript.

REFERENCES

- Arts, M. G. J. (1978) A mathematical model of the dynamics of the left ventricle and the coronary circulation. Thesis, State University of Limburg.
- Back, L. H. (1977) Left ventricular wall and fluid dynamics of cardiac contraction. *Math. Biosci.* **36**, 257–297.
- Guntheroth, W. G. (1974) Changes in left ventricular wall thickness during the cardiac cycle. *J. appl. Physiol.* **36**, 308–312.
- Hort, W. (1960) Makroskopische und mikrometrische Untersuchungen am Myocard verschieden stark gefüllter linker Kammern. *Virchows Arch. (Pathol. Anat.)* **333**, 523–564.
- Huxley, A. F. (1957) Muscle structure and theories of contraction. *Prog. Biophys. Biophys. Chem.* **7**, 255–318.
- Mirsky, J. (1970) Effects of anisotropy and nonhomogeneity on left ventricular stresses in the intact heart. *Bull. math. Biophys.* **32**, 197–213.
- Pollack, G. H. and Krueger, J. W. (1976) Sarcomere dynamics in intact cardiac muscle. *Eur. J. Cardiol.* **4**, suppl. 53–65.
- Rankin, J. S., MacHall, P. A., Arentzen, C. E., Ling, D., Greenfield, J. C. and Anderson, R. W. (1976) The three dimensional dynamic geometry of the left ventricle in the conscious dog. *Circ. Res.* **39**, 304–313.
- Ross, J. Jr., Sonnenblick, E. H., Covell, J. W., Kaiser, G. A. and Spiro, D. (1967) The architecture of the heart in systole and diastole. *Circ. Res.* **21**, 409–421.
- Ross, M. A. and Streeter, D. D. Jr. (1975) Nonuniform subendocardial fibre orientation in the normal macaque left ventricle. *Eur. J. Cardiol.* **3/3**, 229–247.
- Sandler, H. (1970) Dimensional analysis of the heart. *Am. J. Med. Sci.* **260**, 56–70.
- Sandler, H. and Alderman, E. (1974) Determination of left ventricular size and shape. *Circ. Res.* **34**, 1–8.
- Sasayama, S., Franklin, D., Ross, J. Jr., Kemper, W. A. and McKown, D. (1976) Dynamic changes in left ventricular wall thickness and their use in analyzing cardiac function in the conscious dog. *Am. J. Cardiol.* **38**, 870–879.
- Sonnenblick, E. H. and Skelton, C. L. (1974) Reconsideration of the ultrastructural basis of cardiac length-tension relations. *Circ. Res.* **35**, 514–526.
- Spotnitz, H. M., Sonnenblick, E. H. and Spiro, D. (1966) Relation of ultrastructure to function in the intact heart: sarcomere structure relative to pressure volume curves of intact left ventricles of dog and cat. *Circ. Res.* **18**, 49–66.
- Streeter, D. D. Jr., Spotnitz, H. M., Patel, D. P., Ross, J. Jr. and Sonnenblick, E. H. (1969) Fibre orientation in the canine left ventricle during diastole and systole. *Circ. Res.* **24**, 339–347.
- Streeter, D. D. Jr., Vaishnav, R. N., Patel, D. J., Spotnitz, J. M., Ross, J. Jr. and Sonnenblick, E. H. (1970) Stress distribution in the canine left ventricle during diastole and systole. *Biophys. J.* **10**, 345–363.
- Streeter, D. D. Jr. and Hanna, W. T. (1973a) Engineering mechanics for successive states in canine left ventricular myocardium: I. Cavity and wall geometry. *Circ. Res.* **33**, 639–655.
- Streeter, D. D. Jr. and Hanna, W. T. (1973b) Engineering mechanics for successive states in canine left ventricular myocardium: II. Fibre angle and sarcomere length. *Circ. Res.* **33**, 656–664.
- Suga, H. and Sagawa, K. (1974) Assessment of absolute volume from diameter of the intact left ventricular cavity. *J. appl. Physiol.* **36**, 496–499.
- Van den Broek, J. H. J. M. and Denier van der Gon, J. J. (1980a) A Model for Left Ventricular Contractions Based on the Sliding Filament Theory. *Cardiac Dynamics*. (Edited by Baan, J., Arntzenius, A. C. and Yellin, E. L.), pp. 135–142. Martinus Nijhoff, The Hague.
- Van den Broek, J. H. J. M. and Denier van der Gon, J. J. (1980b) A model study of isovolumic and non-isovolumic left ventricular contractions. *J. Biomechanics* **13**, 77–87.
- Wong, A. Y. K. (1973) Myocardial mechanics: application of sliding-filament theory to isovolumic contraction of the left ventricle. *J. Biomechanics* **6**, 565–581.
- Yoran, C., Covell, J. W. and Ross, J. Jr. (1973) Structural basis for the ascending limb of left ventricular function. *Circ. Res.* **32**, 297–303.

APPENDICES

A. Pressure in the apex of a general ellipsoid

Suppose in a certain wall layer at the apex of a general ellipsoid the radius of curvature in the x - z plane is denoted R_1 and the one in the y - z plane R_2 . Approaching the apex from a line of longitude within this layer lying in the x - z plane and from a similar line lying in the y - z plane, the pressure increments over the wall layer converge to:

$$\sigma_m \left(\frac{\cos^2 \phi}{R_2} + \frac{\sin^2 \phi}{R_1} \right) du \quad \text{and} \quad (A1)$$

$$\sigma_m \left(\frac{\cos^2 \phi}{R_1} + \frac{\sin^2 \phi}{R_2} \right) du$$

respectively.

Sine σ_m , du and ϕ converge to the same value in the apex, these two expressions are equal only if $\phi = \pm 45^\circ$, which is probably not true in every apical wall layer, or if $R_1 = R_2$, which means that the ellipsoid is an ellipsoid of revolution in the apex.

B. Calculations needed to determine ventricular pressure, fibre length and orientation

The radii of curvature. In the literature expressions for r and R are given in spherical coordinates (Mirsky, 1970). Conversion to a rectangular frame leads to the following expression for the radii in a point (x, y, z) on an ellipsoid with axes (b, b, a) :

$$r = \left(x^2 + y^2 + \left(\frac{b}{a} \right)^4 z^2 \right)^{1/2}$$

$$R = \frac{a^2}{b^4} \left(x^2 + y^2 + \left(\frac{b}{a} \right)^4 z^2 \right)^{3/2}. \quad (A2)$$

Division of the wall into wall layers. $V(E_i)$ is the volume enclosed by E_i and is given by:

$$V(E_i) = Bb_i^3 a_i,$$

with

$$B = \frac{\pi}{3} (2 + 3k - k^3). \quad (A3)$$

If $V_{w,i}$ is the wall volume (minus V_a) between E_i and E_0 , the extra volume $V_{e,i}$ resulting from the special way of truncating the ellipsoid (see Fig. 3) is defined as:

$$V_{e,i} = V(E_i) - V(E_0) - V_{w,i}. \quad (A4)$$

$V_{e,i}$ can be expressed in the axes of E_i and E_0 by:

$$V_{e,i} = \frac{\pi}{3}(k - k^3)(a_i - a_0)(b_i^2 + b_0^2 + b_i b_0). \quad (A5)$$

In the reference situation the wall is divided into equidistant layers with the aid of ellipsoids E_i , so that:

$$\begin{aligned} b_i &= b_0 + (b_m - b_0) \frac{i}{m} \\ a_i &= a_0 + (a_m - a_0) \frac{i}{m}. \end{aligned} \quad (A6)$$

After deformation we get, since $V_{w,i}$ is supposed to be constant,

$$\begin{aligned} V(E'_i) - V(E'_0) - V'_{e,i} \\ = V(E_i) - V(E_0) - V_{e,i} = V_{w,i}, \end{aligned} \quad (A7)$$

where apostrophes denote the deformed state.

The axes of E'_i can be expressed in terms of those of E_0 by:

$$\begin{aligned} b'_i &= b'_0 + x_i \\ a'_i &= a'_0 + z_i. \end{aligned} \quad (A8)$$

Deformation is supposed to take place such that $z_i = wx_i$, with:

$$w = (a'_m - a'_0)/(b'_m - b'_0).$$

Equation (A7) can now be rewritten as a third order algebraic equation in x_i which can be solved analytically or numerically:

$$y_i^3 + 3py_i + 2q = 0, \quad (A9)$$

with

$$\begin{aligned} y_i &= x_i + \frac{\gamma}{3\delta} \\ p &= \frac{\beta}{3\delta} - \frac{\gamma^2}{9\delta^2} \\ q &= \frac{\gamma^3}{27\delta^3} - \frac{\beta\gamma}{6\delta^2} + \frac{\alpha - C}{2\delta}, \end{aligned}$$

and

$$\begin{aligned} \alpha &= B(b'_0)^2 a'_0 \\ \beta &= B(b'_0)^2 w + 2Ba'_0 b'_0 - 3A(b'_0)^2 \\ \gamma &= Ba'_0 + 2Bb'_0 w - 3Ab'_0 \\ \delta &= Bw - A, \end{aligned}$$

where B is given by (A3) and A and C by:

$$\begin{aligned} A &= \frac{\pi}{3}(k - k^3)w \\ C &= V(E_i) - V(E_0) - V_{e,i} + V(E'_0). \end{aligned}$$

Determination of the wall thickness Δu_i . $S(x, y, z)$ is a point on E_0 . Δu_i is the length between E_{i-1} and E_i measured along the normal N through S . The direction vector of N , called \mathbf{n} can be obtained by taking the gradient of the level (equipotential) surface

$$\left(\frac{x^2}{b_0^2} + \frac{y^2}{b_0^2} + \frac{z^2}{a_0^2} \right).$$

So:

$$\mathbf{n} = \left(\frac{x}{b_0^2}, \frac{y}{b_0^2}, \frac{z}{a_0^2} \right). \quad (A10)$$

N can now be represented by the vector equation:

$$\mathbf{N} = \mathbf{x} + \lambda \mathbf{n}, \quad (A11)$$

with $\mathbf{x} = (x, y, z)$.

Intersection of N with E_i results in:

$$\frac{(x^2 + y^2)}{b_i^2} \left(1 + \frac{\lambda_i}{b_0^2} \right)^2 + \frac{z^2}{a_i^2} \left(1 + \frac{\lambda_i^2}{a_0^2} \right)^2 = 1. \quad (A12)$$

From the two solutions of λ the positive one has to be chosen. For Δu_i one finds now:

$$\begin{aligned} \Delta u_i &= |\lambda_i \mathbf{n}| - |\lambda_{i-1} \mathbf{n}| \\ &= (\lambda_i - \lambda_{i-1}) \left(\frac{x^2}{b_0^4} + \frac{y^2}{b_0^4} + \frac{z^2}{a_0^4} \right)^{1/2}. \end{aligned} \quad (A13)$$

Determination of fibre length and fibre orientation. Sarcomeres in ellipsoid E are represented by straight lines lying in the tangent planes on E . Since the sarcomere lengths are very small in relation to the dimensions of the ellipsoids, the error introduced by this assumption is negligible. It is supposed that if ellipsoid E with axes (b, b, a) transposes into E' with axes (b', b', a') , the point of contact $P(x, y, z)$ of E and the tangent plane at E transposes into $P'(x', y', z')$ or $P' \left(x \frac{b'}{b}, y \frac{b'}{b}, z \frac{a'}{a} \right)$, while the tangent plane at E transposes to the tangent plane at E' . The tangent plane at E is determined by two linearly independent vectors \mathbf{r}_1 and \mathbf{r}_2 . After deformation \mathbf{r}'_1 and \mathbf{r}'_2 can be obtained by multiplying the x, y and z components of \mathbf{r}_1 and \mathbf{r}_2 by $\frac{b'}{b}, \frac{b'}{b}$ and $\frac{a'}{a}$ respectively. \mathbf{r}_1 is taken parallel to the x - y plane and perpendicular to \mathbf{n} (see equation A10) so that:

$$\mathbf{r}_1 = (-y, x, 0). \quad (A14)$$

\mathbf{r}_2 is taken perpendicular to \mathbf{r}_1 and \mathbf{n} so that:

$$\mathbf{r}_2 = \left(xy, yz, -\frac{a^2}{b^2}(x^2 + y^2) \right). \quad (A15)$$

The muscle fibre in P is now represented by the line element:

$$\mathbf{L} = \mathbf{x} + \lambda \mathbf{s}, \quad 0 \leq \lambda \leq l_m, \quad (A16)$$

with $\mathbf{x} = (x, y, z)$ and l_m the fibre length. The direction vector \mathbf{s} is represented by:

$$\mathbf{s} = \frac{\mathbf{r}_1}{|\mathbf{r}_1|} \cos \phi + \frac{\mathbf{r}_2}{|\mathbf{r}_2|} \sin \phi. \quad (A17)$$

This last equation holds true since the maximum length of the line element is given by $|\mathbf{L}|$ which equals l_m , while the cosine of the angle between \mathbf{r}_1 and \mathbf{s} is given by $(\mathbf{r}_1 \cdot \mathbf{s})/|\mathbf{r}_1|$ which equals $\cos \phi$.

After deformation the new line element \mathbf{L}' is given by:

$$\mathbf{L}' = \mathbf{x}' + \lambda \mathbf{s}', \quad 0 \leq \lambda \leq l_m, \quad (A18)$$

with

$$\mathbf{s}' = \frac{\mathbf{r}'_1}{|\mathbf{r}'_1|} \cos \phi + \frac{\mathbf{r}'_2}{|\mathbf{r}'_2|} \sin \phi. \quad (A19)$$

l'_m and ϕ' now become:

$$l'_m = l_m |\mathbf{s}'| \quad (A20)$$

$$\phi' = \arccos \frac{\mathbf{s}' \cdot \mathbf{r}'_1}{|\mathbf{s}'| |\mathbf{r}'_1|}. \quad (A21)$$

C. Modelling of the axis in the reference situation

The following procedure is applied:

- A value for the equatorial wall thickness dx and the apical wall thickness dz is chosen. (A good choice of dz

appears to be $dz = dx(b_0/a_0)$. The outer axes can now be represented by:

$$b_m = b_0 + dx, \quad \text{and} \quad a_m = a_0 + dz, \quad (\text{A22})$$

and thus inner axes by:

$$b_0 = \left(\frac{V_0 + V_q - V_e}{Bd_r} \right)^{1/3}, \quad \text{and} \quad a_0 = b_0 d_r. \quad (\text{A23})$$

where B is given by equation (A3) and V_e by equation (A5) for $i = m$. Since V_e depends on the unknown E_m , in first instance it is neglected here. The pressure at the equator P_E and at the apex P_A are calculated. Both pressures depend on b_m and a_m .

- b. A new value of a_m called a'_m is found by changing dz iteratively such that $P_E(b_m, a'_m)$ equals $P_A(b_m, a_m)$.
- c. If $P_A(b_m, a'_m)$ equals $P_A(b_m, a_m)$ we go to step d. If not we go back to b with the new value of P_A .
- d. Use the newly obtained axes of E_m to check whether the wall volume V_w (equation 8) is correct within the desired accuracy. If not, a new estimate of dx is chosen and steps a to d are repeated.
- e. V_e can now be calculated from E_m and E_0 . New values of b_0 and a_0 follow from V_e (equation A23). Procedures a to d are repeated until two successive approximations of E_0 agree satisfactorily.

The iterative procedures in b, d and e are executed numerically with a secant-method.

D. Modelling of the axes at another preload

The inner axes follow from equation (A23) in which V_0 , d_r , b_0 and a_0 are replaced by V_p , d , b'_0 and a'_0 respectively. Again V_e is neglected in the first instance, this is corrected iteratively afterwards. The outer axes are represented by:

$$b'_m = b'_0 + dx, \quad \text{and} \quad a'_m = a'_0 + w dx, \quad (\text{A24})$$

where w is given and dx is unknown. From the constancy of the wall volume, dx can be determined. The resulting set of equations is the same as given in (A9). However, x_i should be replaced by dx and C by:

$$C = V_{w,m} + V(E'_0) \quad (\text{A25})$$

with $V_{w,m} = V_w - V_q$.

E. Modelling of the axes in the ejection phase

For the inner axes and V_e the same procedure as given in

Appendix D holds, but V_p should be replaced by V . For the outer axes it is supposed that:

$$b'_m = b'_0 + dx, \quad \phi \quad \text{and} \quad a'_m = a'_0 + dz, \quad (\text{A26})$$

where dz is given and dx is unknown. The constancy of the wall volume results now in an equation of the second degree in dx :

$$a dx^2 + b dx + c = 0, \quad (\text{A27})$$

with

$$a = B(a'_0 + dz) - A$$

$$b = 2Bb'_0(a'_0 + dz) - 3Ab'_0$$

$$c = B(b'_0)^2(a'_0 + dz) - 3A(b'_0) - C.$$

B and C are given by (A3) and (A25), A is given by:

$$A = \frac{\pi}{3}(k - k^3)dz.$$

NOMENCLATURE

$E_i (i=0,1,\dots,m)$	ellipsoids forming the m layers of the ventricular wall
E_0, E_m	ellipsoids describing the endo- and epicardium
a_i, b_i	long and short (semi-) axes of E_i
k	truncation factor of the ellipsoid
d	ratio between short and long inner axes
d_r	value of d in the reference situation
d_p, d_e	parameters describing the influence of preload and ejection on d respectively
h_E, h_A	wall thickness at the equator and apex respectively
F_m, l_m, ϕ	force, length and orientation of the muscle fibre
r, R	radii of curvature
du	thickness of a wall layer
V_0	inner volume in the reference situation
V_p	inner volume at a different preload
V_e	inner volume during ejection
V_w	wall volume
V_q	papillary muscle volume
V_e	extra volume resulting from the special way of truncating the ellipsoid
$V(E_i)$	volume enclosed by E_i